Dalton Transactions

ROYAL SOCIETY OF CHEMISTRY

PAPER

View Article Online
View Journal | View Issue

Cite this: *Dalton Trans.*, 2025, **54**, 2421

Two-fold proton coupled electron transfer of a Ta(v) aniline complex mediated by a redox active NNN pincer ligand†

Sotirios Pavlidis, Jasmin Alasadi, Amanda Opis-Basilio and Josh Abbenseth *

Received 23rd November 2024,
Accepted 16th December 2024

DOI: 10.1039/d4dt03281k

rsc.li/dalton

We report the proton-coupled electron transfer (PCET) reactivity of an octahedral Ta(v) aniline complex supported by an acridane-derived redox active NNN pincer ligand. The reversible binding of aniline to a Ta(v) dichloride induces significant coordination-induced bond weakening (CIBW) of the aniline N–H bonds. This enables a rare two-fold hydrogen atom abstraction, resulting in a terminal imido complex and a two-electron oxidation of the NNN pincer ligand, all while maintaining the metal's oxidation state. The bond dissociation free energies (BDFEs) of the aniline and a transient radical amido complex are estimated through stoichiometric reactions with different hydrogen atom abstractors and donors, further supported by density functional theory calculations.

Introduction

Proton coupled electron transfer (PCET) reactions are of fundamental importance in biology and essential chemical transformations of small molecules such as CO_2, H_2, NH_3 and many others.[1] In contrast to transition metal hydrides in which PCET leads to ligand loss/gain and oxidation state change of the respective metal centre, the spatial separation of proton and electron donor sites represents an intriguing tool to tune PCET reactions. In selected cases redox active ligands can actively participate in these reaction schemes providing an efficient tool to steer thermodynamic parameters.[2,3] In this context, controlling PCET is vital for the conceptualisation of homolytic N–H cleavage and bond formation reactions which are key processes in ammonia oxidation and N_2 fixation chemistry.[4,5] The corresponding bond dissociation free energies (BDFEs) of metal coordinated N–H moieties are dictated by the respective metal centre *via* coordination induced bond weakening (CIBW).[6] Effective CIBW of X–H bonds usually requires that the transition metal complex is strongly reducing, as demonstrated by recent examples of tremendous weakening of O–H and N–H bond by, *e.g.*, Mo(I/II) or Sm(II), that can even lead to spontaneous formation of dihydrogen in rare cases.[7,8] Consequently, CIBW should be minimal for high valent early transition metal centres that do not feature d-electrons since metal centred electron transfer cannot occur. Within this context, PCET studies on high valent early transition metal complexes ligated by redox active ligands remain rare but hold immense potential for the conceptualisation of novel N_2 reduction and ammonia oxidation schemes since reduced early transition metals display a high propensity to cleave the strong N≡N triple bond to form nitride complexes in high oxidation states.[3c,i,l,5,7d] Chirik and co-workers demonstrated that a V(v) bis-phenylimido complex featuring a redox active pyridine diimine (PDI) radical ligand can undergo PCET to facilitate N–H bond formation (Fig. 1).[3i] Upon conversion of an imido towards an amido ligand, the PDI radical ligand is reduced to its dianionic state. A second PCET process forms the corresponding bis-amido complex associated with regeneration of the monoanionic radical state of the PDI ligand and two-electron reduction of the metal centre. This demonstrates the vast potential of redox active ligands in N–H bond formation schemes involving high valent early transition metals. Heyduk and co-workers have demonstrated that Ta(v) complexes ligated by diphenylamide-derived NNN pincer ligands can undergo one- and two-electron redox reactions accompanied by oxidation of the pincer ligand, even allowing for catalytic applications.[9] This also included the oxidation of a $[TaCl_2(NNN^{cat})]$ complex by phenyl azide to give an imido complex accompanied by two-electron oxidation of the pincer ligand (Fig. 1).[9b] We recently reported the synthesis of the Ta(v) dichloride **I** and its reactivity towards dioxygen to give the dinuclear biradical complex **II** (Fig. 1).[10] The utilisation of an acridane-derived redox active pincer ligand allowed for the prior unprecedented full four-electron reduction of O_2 by a transition metal complex without any d-electrons. In analogy

Institut für Chemie, Humboldt-Universität zu Berlin, Brook-Taylor-Str. 2, 12489 Berlin, Germany. E-mail: josh.abbenseth@hu.berlin.de

†Electronic supplementary information (ESI) available: Synthetic procedures and additional spectroscopy, details on performed DFT calculations and crystallographic information. CCDC 2383359, 2383360 and 2402128. For ESI and crystallographic data in CIF or other electronic format see DOI: https://doi.org/10.1039/d4dt03281k

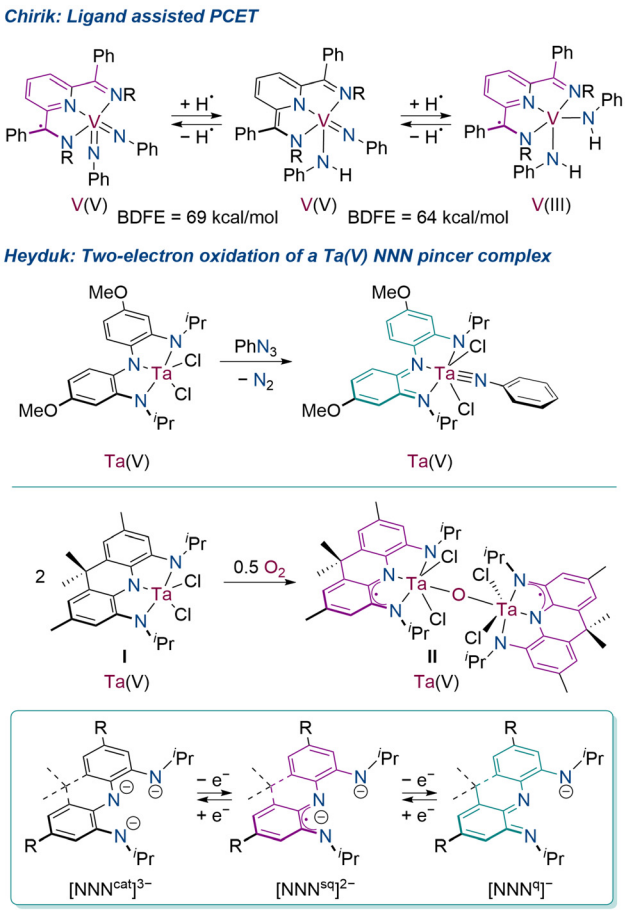

Fig. 1 Interconversion of vanadium PDI complexes *via* PCET (top, calculated BDFE values given) and two-electron oxidation of a $TaCl_2$(NNN) complex by phenyl azide (middle); recent report on dioxygen splitting by **I** and the three possible oxidation states of the utilised redox active NNN pincer ligand (bottom; cat = catecholate, sq = semiquinone, q = quinone; R = OMe, Me).

to Heyduk's ligand platform, we demonstrated that the ligand cycles through all three accessible oxidation states (labelled as cat, sq and q, Fig. 1) over the course of this transformation. Inspired by these results and Heyduk's ground-breaking work, we sought to explore whether complex **I**, despite featuring Ta in its highest oxidation state, exhibits sufficient CIBW of N–H bonds to allow for N–H bond oxidation. Here we report the first example of a d^0 configured transition metal complex that displays sufficient CIBW of N–H bonds to mediate two-fold PCET resulting in the formation of a terminal imido complex accompanied by two-electron oxidation of the utilised redox active NNN pincer ligand.

Results and discussion

We successfully developed an improved synthesis of 2,2,7,7-tetramethyl-9,10-dihydroacridine which unlocks large scale access to the NNN pincer protioligand N^4,N^5-diisopropyl-2,2,7,7-tetramethyl-9,10-dihydroacridine-4,5-diamine (^{H3}**NNN**^{cat}) *via* a seven-step synthesis without the need for purification by column chromatography or recrystallisation (see ESI†). In contrast to our prior report, the utilisation of MeLi can be avoided in combination with the possibility to upscale the reaction to >10 g. When freshly prepared [$TaCl_2$(NNN^{cat})][9] (**I**), generated *via* reaction of ^{H3}**NNN**^{cat} with $TaMe_3Cl_2$ in toluene at 100 °C, is reacted with one equivalent of aniline in toluene, a minor broadening and shift of the complex's resonances in the ^{1}H NMR spectrum is observed (methylene proton of the isopropyl group shifts by $\Delta\delta_H$ = 0.6 ppm). Upon gradual cooling of a solution of **I** and aniline in dichloromethane, a further signal broadening can be observed for the aniline ligand, as well as for the axial methyl groups of the pincer ligand while the other pincer signals remain sharp. At −40 °C, clean formation of a C_S symmetric diamagnetic compound can be observed, indicative of reversible coordination of aniline to give [$TaCl_2${N(Ph)H_2}{NNN^{cat}}] (**1**, Fig. 2). Determination of this reaction's equilibrium constant

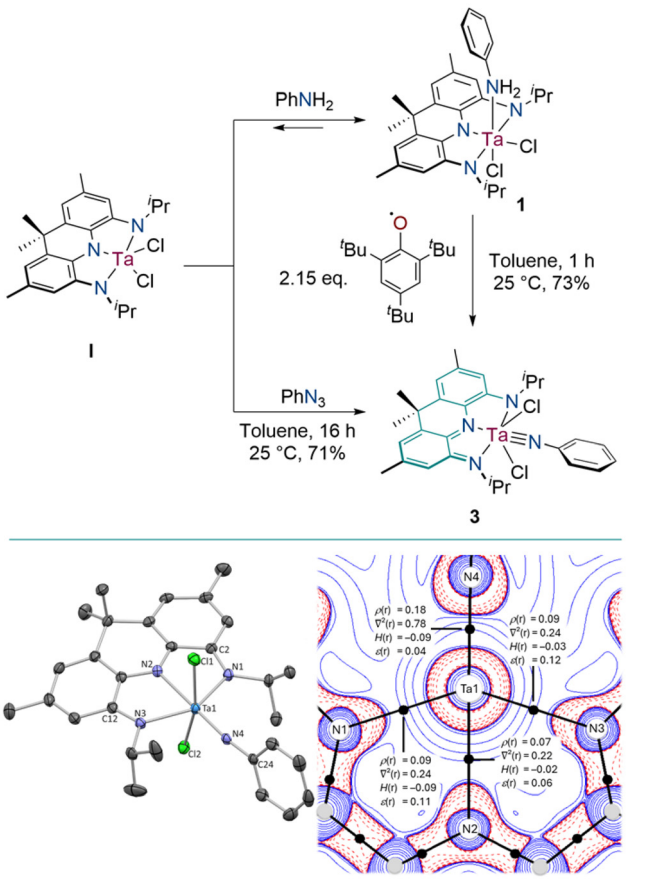

Fig. 2 Reactivity of **I** towards $PhNH_2$ and PhN_3 to produce **1** and **3**, respectively, and PCET to convert **1** into **3** (top); molecular structure of **3** derived by SCXRD (bottom left), solvent molecules and hydrogen atoms removed for clarity; ellipsoids at 50% probability level; bond lengths in Å, angles in °: Ta1–N1 2.158(2); Ta1–N2 2.218(2); Ta1–N3 2.153(2); Ta1–N4 1.79(1); Ta1–Cl1 2.4343(8); Ta1–Cl2 2.4283(7); N1–C2 1.345(4); N3–C12 1.354(4); Ta1–N4–C24 174(1); N2–Ta1–N4 179.2(4); QTAIM analysis of Ta–N bonding in **3** (bottom right).

was hindered by partial amorphous precipitation of **1** at low temperatures in toluene, DCM and THF. We have previously reported that the redox active NNN pincer ligand can be oxidised by one as well as two electrons suggesting that PCET to give the amido radical complex [$TaCl_2${N(Ph)H}{NNN^{sq}}] (**2**) and ultimately the imido complex [$TaCl_2${N(Ph)}{NNN^{q}}] (**3**) might be feasible.[10] PCET reactivity of **1** was tested upon reaction with 2.15 eq. of the hydrogen atom abstraction agent 2,4,6-tris(*tert*-butyl)phenoxy-radical (Ph*O$^{\bullet}$). Upon mixing, an immediate reaction is evidenced by a rapid colour change of the reaction mixture towards dark green. The ^{1}H NMR spectrum shows quantitative formation of two equivalents of 2,4,6-tris-*tert*-butylphenol (Ph*OH) and a new diamagnetic Ta complex.

The latter exhibits C_{2v} symmetry on the NMR timescale and features characteristic resonances of a singly substituted phenyl ring in addition to the signals of the acridane NNN pincer ligand suggesting formation of the desired imido complex **3**. When **I** is reacted with one equivalent of phenyl azide in toluene at room temperature overnight, clean formation of the identical product is observed by NMR spectroscopy. Single crystal X-ray diffraction (SCXRD) confirms the expected speciation of the imido complex **3** which features a Ta(v) centre in a distorted octahedral coordination sphere (Fig. 2). An alternative synthetic access towards **3** upon reaction of **I** with diazobenzene proved to be unsuccessful. The Ta–N_{imido} bond (1.79(1) Å) is comparably short and best described as a triple bond since two π-bonding interactions can be realised towards the d^0 configured metal centre. This is further supported by a calculated ellipticity of the Ta≡NPh bond of 0.04 and a distinctively higher Laplacian of electron density at the bond critical point derived *via* quantum theory of atoms in molecules (QTAIM)[11] calculations relative to the Ta–N_{ligand} bonds (Fig. 2). In addition, the Ta–N_{ligand} bond lengths are considerably elongated when compared to **I**.[10] The NNN pincer ligand exhibits clear signs of two-electron oxidation due to a significant shortening of the $N_{1/3}$–$C_{2/12}$ bonds within the ligand compared to **I** or ^{H3}**NNN**^{cat}. Furthermore, the aromatic C–C bonds show more pronounced localisation of double and single bonds in line with the increased quinone character of the two-electron oxidised ligand (Table S10†).‡ These values compare well with prior reported Ta(v) complexes which feature structurally related two-electron oxidised NNN pincer ligands as well as recently reported Bi complexes that leverage the redox activity of acridane-derived NNN pincer scaffolds.[9,10,12] The two-fold PCET reactivity of **1** demonstrates that the N–H BDFE of aniline can be effectively lowered by over 10 kcal mol^{-1} upon reversible CIBW by the Ta(v) complex **I**

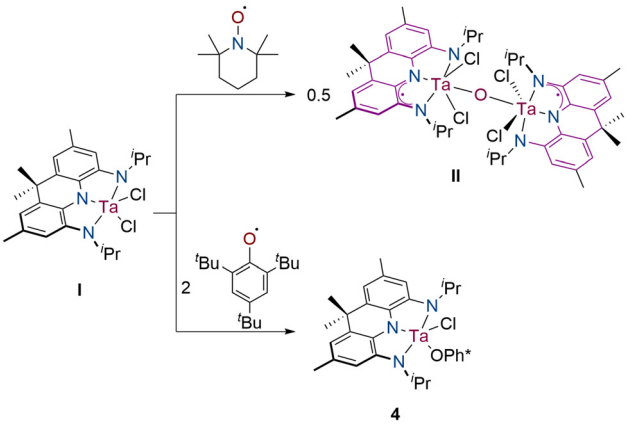

Fig. 3 Reactivity of **I** towards hydrogen atom abstractors employed in this study in the absence of aniline.

(BDFE($PhNH_2$): 86.0 kcal mol^{-1}; BDFE(Ph*OH): 75.5 kcal mol^{-1}).[1b,§]

When **1** is reacted with one equivalent of the 2,2,6,6-tetramethylpiperidinyloxyl radical (TEMPO$^{\bullet}$, BDFE(TEMPOH): 63.8 kcal mol^{-1})[1b] in toluene, ^{1}H NMR spectroscopy indicates that no PCET but rather oxygen atom transfer occurs to produce the prior reported binuclear oxo complex **II** accompanied by the release of aniline. Consequently, the reaction of **I** with TEMPO$^{\bullet}$ also yields **II** (Fig. 3) due to tantalum's inherent high oxophilicity and the significant thermodynamic driving force to form a Ta–O–Ta moiety as recently reported by us.[10] Interestingly, **I** also reacts with two equivalents of Ph*O$^{\bullet}$ in the absence of aniline to cleanly produce a diamagnetic complex which features C_S symmetry on the ^{1}H NMR timescale and one equivalent of Ph*OH. SCXRD reveals the formation of the Ta(v) complex [TaCl(Ph*O)(NNN^{cat})] (**4**, Fig. 3) in which the Ta centre adopts a trigonal bipyramidal coordination geometry. The bond lengths around the metal centre as well as the C–C and C–N bond lengths within the pincer ligand confirm the presence of the fully reduced catecholate ligand oxidation state when compared to ^{H3}**NNN**^{cat} and **I** (see ESI†).

Further insights about the relative margin of the two N–H BDFEs associated with the conversion of **1** to **2** and **3** were obtained *via* reaction of **1** with one equivalent of Ph*O$^{\bullet}$. At room temperature, an instant colour change towards dark brown is observed. The ^{1}H NMR spectrum shows the clean formation of the imido complex **3** in 50% spectroscopic yield accompanied by 50% of unreacted **1**. Consequently, the BDFE of **2** is considerably lower than that of **1**. When **3** is treated with an excess of TEMPOH no reaction is observed *via* ^{1}H NMR spectroscopy indicating that the BDFE of **2** is lower than 63.8 kcal mol^{-1}.[1b] To derive more information about the associated thermodynamical square scheme of the second PCET process and to possibly access the radical complex **2**, **3**

‡The experimental bond distances indicate that both arms of the NNN pincer ligand exhibit identical C–C and C–N bond lengths, preserving symmetry even upon one- or two-electron ligand-centred oxidation. To clearly illustrate the ligand-centred oxidation in the Ta complexes, we chose to represent the chemical structures with asymmetrical ligands, enhancing the visual communication of this feature to the reader.

§Since no BDFE values for TEMPOH and Ph*OH in toluene are available we refer to the reported values in benzene throughout the manuscript.

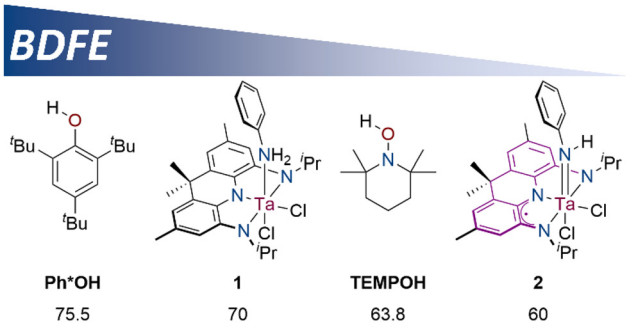

Fig. 4 BDFE values of used reagents and calculated values for **1** and **2**. BDFE values of TEMPOH and Ph*OH adapted from ref. 1*b*; computational method: D3BJ-RIJCOSX-PBE0/def2-TZVP/CPCM(benzene)//D3BJ-RIJCOSX-PBE0/def2-SVP(def2-TZVP{Cl,N,Ta}).

was characterised *via* cyclic voltammetry in tetrahydrofuran. A quasi-reversible one-electron reduction is observed at $E_{1/2}$ = −0.85 V *vs.* $Fc^{0/+}$ (see ESI†). Attempted reduction with $CoCp_2$ in DCM however results in unselective decomposition. Similarly, when **3** is reduced by KC_8/222-crypt in THF at −30 °C (222-crypt = 4,7,13,16,21,24-hexaoxa-1,10-diazabicyclo[8.8.8] hexacosane) no formation of a paramagnetic complex is observed. An alternative synthetic access towards **2** is represented by initial protonation of **3** followed by one-electron reduction. When **3** is reacted with one equivalent of $[H(OEt_2)_2][BArF_{24}]$ ($BArF_{24}$: $\{B(3,5\text{-}CF_3\text{-}C_6H_3)_4\}^-$) in DCM or in a toluene/ether mixture at low temperatures, unselective decomposition is observed as well rendering both methodologies unsuitable to generate **2**. We utilised DFT calculations to obtain further insights into the respective BDFE values as well as the electronic structure of the fleeting radical complex **2**. The calculated spin density of **2** is mainly located on the NNN pincer ligand with negligible contributions of the metal centre which aligns with prior reported Ta(v) complexes ligated by open-shell pincer ligands (see ESI†).[9,10] The DFT-calculated values for BDFE(**1**) and BDFE (**2**) are 70 kcal mol^{-1} and 60 kcal mol^{-1}, respectively, demonstrating a considerable CIBW of aniline's N–H bonds despite Ta being in its highest oxidation state (Fig. 4).

These BDFE values yield a positive comproportionation free energy of **1** and **3** to give **2** (ΔG_{DFT} = +8.4 kcal mol^{-1}). This renders this complex to be inaccessible *via* a PCET route which is fully consistent with our experimental findings.

To further substantiate our claim that **2** is a viable transient intermediate in the oxidation of **1** towards **3**, we attempted to generate a mononuclear Ta(v) complex featuring a dianionic radical NNN^{sq} pincer ligand thereby providing a series of mononuclear Ta(v) complexes ligated by the NNN ligand in all three possible oxidation states. Reaction of **I** with iodobenzene dichloride leads to a gradual colour change from red to purple. SCXRD confirms the formation of the radical complex **5** which was obtained in 36% isolated yield and fully characterized by combustion analysis, NMR, UV/vis and IR spectroscopy (Fig. 5, see ESI†). When the pincer ligand undergoes stepwise

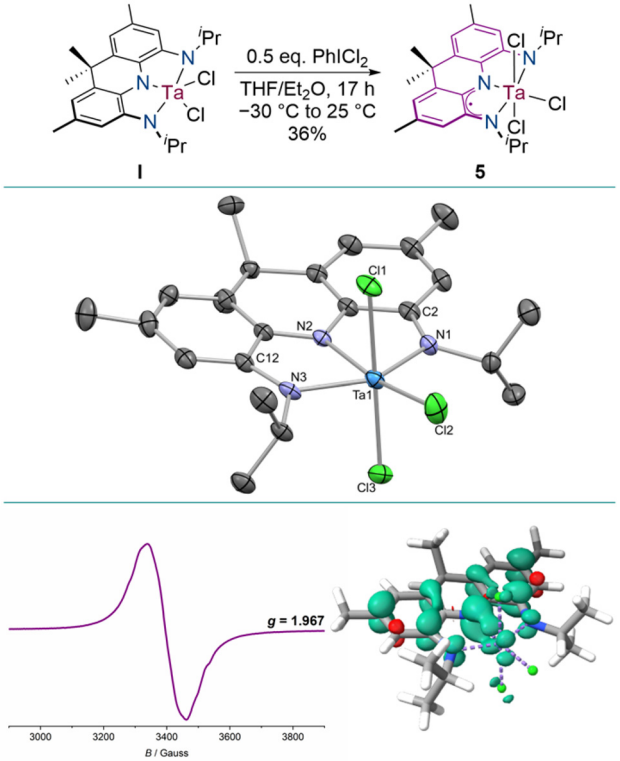

Fig. 5 Synthesis of **5** *via* one-electron oxidation of **I** (top); molecular structure of **5** derived by SCXRD (middle), one complex molecule of the asymmetric unit shown, solvent molecules and hydrogen atoms removed for clarity; ellipsoids at 50% probability level; bond lengths in Å, angles in °: Ta1–N1 2.028(4); Ta1–N2 2.136(3); Ta1–N3 2.025(4); Ta1–Cl1 2.4284(12); Ta1–Cl2 2.3747(12); Ta1–Cl3 2.3767(12); N1–C2 1.371(5); N3–C12 1.373(6); EPR spectrum of **5**, 2.5 mM toluene, 25 °C (bottom left); calculated spin density of **5** (computational method: D3BJ-RIJCOSX-PBE0/def2-TZVP/CPCM(benzene)//D3BJ-RIJCOSX-PBE0/def2-SVP(def2-TZVP{Cl,N,Ta})).

oxidation, the $N_{1/3}$–$C_{2/12}$ bonds become shorter, while the Ta–$N_{1/2/3}$ bonds get longer compared to compounds **I** or **4**. This change aligns with the ligand gaining a semiquinone-like character during oxidation, although this effect is less pronounced than the quinone oxidation state seen in compound **5** (Table S10†).[10] Ligand centred oxidation is further confirmed by EPR spectroscopy in toluene at room temperature. A broadened signal at g = 1.967 is detected indicating the presence of a ligand centred radical, in accord with the calculated spin density of **5** that only displays minor metal contribution (Fig. 5, see ESI†). In contrast to structurally related Ta radical complexes reported by Heyduk and co-workers, no Ta hyperfine interaction could be resolved.[9]

Conclusions

In conclusion, we report a rare example of N–H bond oxidation *via* two-fold PCET at a d^0 configured Ta(v) aniline complex mediated by a redox active NNN pincer ligand. CIBW bond weakening of N–H bonds by at least 10 kcal mol^{-1} is observed

despite the metal being in its maximum oxidation state. Stoichiometric reactions with hydrogen atom abstractors reveal that the second PCET step is associated with a lower N–H BDFE preventing the synthesis of an amido radical complex which was further confirmed by density functional theory. These findings highlight the significant potential of redox-active pincer ligands for developing future catalytic applications, *e.g.*, ammonia oxidation and dinitrogen fixation schemes that leverage pincer ligand assisted PCET steps.

Experimental

Materials and methods

All experiments with air-sensitive compounds were carried out in a glovebox or in a fume hood employing Schlenk techniques under a dry Ar atmosphere. Traces of water and oxygen were removed *via* heating of glassware under vacuum prior to use. All solvents except THF were dried and degassed by a MBraun solvent purification system. THF was dried over sodium, distilled and stored over molecular sieves. Deuterated solvents were degassed *via* three freeze–pump–thaw cycles and stored over molecular sieves. NMR spectra were recorded on AVANCE II 300 MHz, Bruker Avance 400 MHz and Bruker Avance III 500 MHz NMR spectrometers. Chemical shifts are referenced to the signal of residual protonated solvent. IR spectra were recorded on a Bruker ALPHA spectrometer with an ATR sampling unit. Elemental analyses were performed with a HEKA Euro 3000EA elemental analyzer.

UV-vis-spectra were measured in a 1 cm quartz cuvette using an Agilent 8453 UV-vis-spectrophotometer with an Unisoku USP-203-A cryostat. Cyclic voltammetry was performed in a glovebox with a PalmSens Emstat3+ Blue potentiostat using a glassy carbon working electrode, a Pt wire as counter electrode and an Ag wire as pseudo-reference electrode. Continuous wave (CW) X-band electron paramagnetic resonance (EPR) spectra were collected on a Bruker EMXplus Instrument at a frequency of ~9.64 GHz (X-band) in perpendicular polarization mode. All samples for qualitative analysis were measured at room temperature. All commercially available chemicals were used without purification unless otherwise noted. Aniline was distilled, degassed and stored over 4 Å molecular sieve. 2,4,6-Tris-*tert*-butylphenoxyl radical, phenyl azide, $TaMe_3Cl_2$, Brookhart's acid ($[H(OEt_2)_2][BArF_{24}]$) and 2,2,6,6-tetramethyl-1-hydroxypiperidine (TEMPOH) were synthesised according to literature procedures.[13–18]

Synthetic procedures

The ESI† contains a new large-scale synthesis of the pincer protioligand 2,2,7,7-tetramethyl-9,10-dihydroacridine (^{H3}**NNN**^{cat}) and additional information for the experiments discussed in this manuscript. Please see the ESI† for further details.

In situ generation of I

I is generated *in situ* and directly used for further reactivity due to instability when exposed to vacuum for a long time or stored as a solid. Typical procedure for NMR scale reactions: ^{H3}**NNN**^{cat} (10.0 mg, 28.5 μmol, 1.0 eq.) is dissolved in toluene-d_8 (0.3 mL) and added to a solution of $TaMe_3Cl_2$ (8.5 mg, 28.45 μmol, 1.0 eq.) in toluene (0.2 mL). Heating the reaction solution to 100 °C for 1 h results in gas evolution and a bright red colour. The generation of **I** is verified *via* NMR-spectroscopy and in accord with literature. Formed methane is detected at δ = 0.18 ppm.[10]

In situ generation of 1

^{H3}**NNN**^{cat} (10.0 mg, 28.5 μmol, 1.0 eq.) is dissolved in toluene-d_8 (0.3 mL) and added to a solution of $TaMe_3Cl_2$ (8.5 mg, 28.45 μmol, 1.0 eq.) in toluene (0.2 mL). Heating the reaction solution to 100 °C for 1 h results in gas evolution and a bright red colour. Addition of respectively one or two equivalent(s) of aniline results in a red/brown solution as well as some precipitation. Removing the solvent under reduced pressure and immediately re-dissolving in DCM-d_2 leads to a brown, red solution which is examined *via* NMR-spectroscopy (Fig. S6–S9†). Single-crystals suitable for X-ray diffraction could not be measured due to facile decoordination of aniline and loss of crystallinity during the picking and mounting process.

NMR: (CD_2Cl_2, −40 °C): ^{1}H (400 MHz) δ (ppm) = 6.87 (br. s, 3H, $C_{26/27/29}H$), 6.49 (br. s, 4H, NH_2 + $C_{25/29}H$, superimposed), 6.17 (s, 2H, $C_{5/9}H$), 4.98 (s, 2H, NH_2), 4.89 (hept, J = 6.8 Hz, 2H, $C_{14/17}H$), 2.38 (s, 6H, C_7CH_3), 1.49 (s, 3H, $C_{4/10}CH_3$), 1.36 (d, J = 6.7 Hz, 6H, $C_{14/17}CH_3$), 1.31 (s, 3H, $C_{4/10}CH_3$), 1.18 (d, J = 6.9 Hz, 6H, $C_{14/17}CH_3$).

Synthesis of 3

Route A. To a solution of freshly prepared **I** (85.4 mg, 142 μmol, 1.0 eq.) in toluene, aniline (13.0 μL, 142 μmol, 1.0 eq.) is added and stirred for 15 min at 25 °C until some precipitation formed. The red-brown suspension is treated with 2,4,6-tris-*tert*-butylphenoxyl radical (80.0 mg, 306 μmol, 2.15 eq.) and stirred for 16 h at 25 °C. The green reaction suspension is extracted with DCM and the solvent is removed under reduced pressure. Washing with hexane (5 × 5 mL) and removing residual solvent under reduced pressure gives **3** as microcrystalline green powder (71.2 mg, 103 μmol 73%).

Route B. To a solution of freshly prepared **I** (85.4 mg, 142 μmol, 1.0 eq.) in toluene, phenyl azide (15.6 μL, 142 μmol, 1.0 eq.) is added and stirred for 19 h at 25 °C. The green reaction suspension is extracted with DCM and the solvent is removed under reduced pressure. Washing with hexane (5 × 5 mL) and removing residual solvent under reduced pressure gives **3** as a microcrystalline green powder (69.7 mg, 101 μmol, 70.9%).

NMR: (CD_2Cl_2, 25 °C): ^{1}H (500 MHz) δ (ppm) = 7.42–7.34 (m, 2H, $C_{25/29}H$), 7.27 (dd, J = 8.5, 1.3 Hz, 2H, $C_{26/28}H$), 7.00 (d, J = 1.2 Hz, 2H, $C_{3/11}CH$), 6.94 (d, J = 1.1 Hz, 2H, $C_{5/9}H$), 6.92 (tt, J = 7.4, 1.1 Hz, 1H, $C_{27}H$), 4.92 (hept, J = 6.6 Hz, 2H, $C_{14/17}H$), 2.44 (d, J = 1.1 Hz, 6H, $C_{4/10}CH_3$), 1.68 (s, 6H, C_7CH_3), 1.65 (d, J = 6.6 Hz, 12H, $C_{14/17}CH_3$); ^{13}C{^{1}H} (126 MHz) δ (ppm) = 161.45 ($C_{2/12}$), 156.65 (C_{24}), 149.32 ($C_{4/10}$), 141.24 ($C_{1/13}$), 137.10 ($C_{1/13}$), 128.38 ($C_{25/29}$), 128.04 ($C_{26/28}$), 125.38 ($C_{3/11}$), 123.76

(C_{27}), 114.16 ($C_{21/22}$), 54.94 ($C_{14/17}$), 38.91(C_7), 33.90 ($C_{21/22}$), 24.55 ($C_{15/16/18/19}$), 23.94 ($C_{20/23}$). *The ESI† contains a scheme depicting the labelling of carbon atoms*. IR: (ATR, solid, 25 °C): ν (cm^{-1}): 2969 (w), 1482 (m), 1211 (s), 1125 (m), 831 (m) 563 (m). UV/vis: (DCM; 5×10^{-5} M, 25 °C): λ_{max} (nm) = 900, 820, 450, 420, 390. Elem. Anal. found (calcd) for $C_{29}H_{35}Cl_2N_4Ta$: C, 50.09 (50.37); H, 5.10 (5.1); N, 7.88 (8.1).

Reactivity of 1 towards hydrogen atom abstracting agents

2,4,6-Tris-*tert*-butylphenoxyl radical. To a solution of freshly prepared **I** (17.1 mg, 28.4 μmol, 1.0 eq.) in toluene-d_8 (0.5 mL), aniline (2.6 μL, 28.4 μmol, 1.0 eq.) is added and stirred for 15 min at 25 °C. The red-brown suspension is treated with 2,4,6-tris-*tert*-butylphenoxyl radical (7.4 mg, 28.4 μmol, 1.0 eq.) and examined *via* NMR-spectroscopy revealing the formation of **I** + aniline and **3** in a 1 : 1 : 1 ratio (Fig. S17 and S18†).

TEMPO. To a solution of freshly prepared **I** (17.1 mg, 28.4 μmol, 1.0 eq.) in toluene-d_8 (0.5 mL), aniline (2.6 μL, 28.4 μmol, 1.0 eq.) is added and stirred for 15 min at 25 °C until some precipitation is formed. The red-brown suspension is treated with TEMPO$^{\bullet}$ (4.4 mg, 28.4 μmol, 1.0 eq.) and examined *via* NMR-spectroscopy revealing the formation of **II** and free aniline (Fig. S19†).

Reactivity of I towards hydrogen atom abstracting agents

TEMPO. To a solution of freshly prepared **I** (17.93 mg, 29.9 μmol, 1.0 eq.) in toluene-d_8 (0.5 mL) TEMPO$^{\bullet}$ (4.7 mg, 29.9 μmol, 1.0 eq.) is added and examined *via* NMR-spectroscopy revealing the formation of **II** (Fig. S20†).

2,4,6-Tris-*tert*-butylphenoxyl radical. To a solution of freshly prepared **I** (34.2 mg, 56.9 μmol, 1.0 eq.) in toluene (2 mL) 2,4,6-tris-*tert*-butylphenoxyl radical (31.3 mg, 119.7 μmol, 2.1 eq.) is added resulting in an immediate colour change to dark green. After stirring for 18 h at 25 °C the solvent is removed. The solid residue is re-dissolved in DCM-d_2 and examined *via* NMR-spectroscopy revealing the clean formation of Ph*OH and **4** in a 1 : 1 ratio (Fig. S21–S25†).

NMR: (CD_2Cl_2, 25 °C): ^{1}H (500 MHz) δ (ppm) = 7.35 (d, J = 2.6 Hz, 1H, $C_{26/28}$ *H*), 7.23 (d, J = 2.6 Hz, 1H, $C_{26/28}$*H*), 7.21 (s, 2H, Ph*OH), 6.61 (s, 2H, $C_{3/11}$*H*), 6.34 (s, 2H, $C_{5/9}$*H*), 5.06 (s, 1H, PhO*H*), 4.63 (hept, J = 6.6 Hz, 2H $C_{14/17}$*H*), 2.36 (s, 9H, $C_{4/10}CH_3$, superimposed with residual toluene), 1.61 (s, 3H, C_7CH_3), 1.60 (s, 9H, Ph*^{t}*Bu*), 1.55 (d, J = 6.5 Hz, 6H, $C_{14/17}CH_3$), 1.54 (s, 3H, C_7CH_3), 1.46 (s, 18H, PhO*H), 1.31 (s, 9H, PhO*H), 1.28 (s, 9H, Ph*^{t}*Bu*, superimposed), 1.27 (d, J = 6.5 Hz, 3H, $C_{14/17}CH_3$, superimposed), 1.07 (s, 9H, Ph^t*Bu*); $^{13}C\{^1H\}$ (126 MHz) δ (ppm) = 159.73 (C_{24}), 151.43 (Ph*OH), 144.18 ($C_{2/12}$), 143.55 ($C_{25/27/29}$), 141.62 (Ph*OH), 138.86 ($C_{25/27/29}$), 138.78 ($C_{1/13}$), 38.73 ($C_{25/27/29}$), 138.06 (toluene), 135.21 (Ph*OH), 131.30 ($C_{6/8}$), 129.63 ($C_{4/10}$), 129.09 (toluene), 128.30 (toluene), 125.38 (toluene), 123.29 ($C_{26/28}$), 122.72 ($C_{26/28}$), 121.87 (Ph*OH), 118.67 ($C_{3/11}$), 110.26 ($C_{5/9}$), 48.47 ($C_{14/17}$), 35.56 (Ph*OH), 35.49 (Ph*O^t*Bu*), 35.22 (Ph*O^t*Bu*), 34.62 (Ph*O^t*Bu*), 34.54 ($C_{21/22}$), 34.52 (C_7), 34.48 (Ph*O^t*Bu*), 32.26 (Ph*O^t*Bu*), 31.96 ($C_{21/22}$), 31.55 (Ph*OH), 31.30 (Ph*OH), 31.27 (Ph*O^t*Bu*), 30.26 (Ph*OH), 21.56 (toluene), 21.33 ($C_{20/23}$), 19.17 ($C_{15/18}$), 17.69 ($C_{16/19}$). *The ESI† contains a scheme depicting the labelling of carbon atoms*.

Synthesis of 5

^{H3}**NNN**^{cat} (62.0 mg, 0.176 mmol, 1.0 eq.) is dissolved in toluene (3 mL) and added to a solution of $TaMe_3Cl_2$ (52.4 mg, 0.176 mmol, 1.0 eq.) in toluene (2 mL). Heating the reaction solution to 100 °C for 1 h results in gas evolution and a bright red colour. After cooling the reaction solution to 25 °C, the solvent is removed under vacuum and the obtained dark red solid immediately re-dissolved in THF (3 mL) and cooled to −35 °C. While stirring the THF solution, a solution of $PhICl_2$ (24.3 mg, 88.2 μmol, 0.5 eq.) in Et_2O (15 mL) is added dropwise. After stirring for 30 min at −35 °C the reaction solution is slowly heated to 25 °C and stirred for an additional 17 h. The solvent is removed under reduced pressure and extracted with toluene (3 × 5 mL), followed by reducing the solvent amount, layering with hexane (30 mL) and storing at −30 °C for 4 d. The obtained precipitate is filtered off at −30 °C, washed with hexane (3 × 4 mL) and dried under vacuum. **4** is obtained as dark violet crystals (40.7 mg, 6.46 μmol, 36%). IR: (ATR, solid, 25 °C): ν (cm^{-1}): 2930 (w) 1270 (m), 1225 (s), 701 (s), 557 (m). UV/vis: (toluene, 5×10^{-5} M, 25 °C): λ_{max} (nm) = 890, 570, 340. Elem. Anal. found (calcd) for ($C_{23}H_{30}Cl_3N_3Ta$)(C_7H_8)$_{0.5}$: C, 46.5 (46.7); H, 5.2 (5.0); N, 6.6 (6.2). Elem. Anal. found (calcd) for ($C_{23}H_{30}Cl_3N_3Ta$): C, 43.1 (43.5); H, 4.4 (4.8); N, 5.9 (6.6). *Since toluene co-crystallises with the complex, residual toluene can be present. Extended drying removes the solvent completely accompanied by loss of crystallinity*.

Crystallography

All single crystals were mounted on a MiTeGen micromount with perfluoroether oil. Data were collected from a shock-cooled single crystal at 100(2) K on a Bruker D8 VENTURE dual wavelength Mo/Cu three-circle diffractometer with a microfocus sealed X-ray tube using a mirror optics as monochromator and a Bruker PHOTON III detector. The diffractometer was equipped with an Oxford Cryostream 800 low temperature device and used MoK_α radiation (λ = 0.71073 Å). All data were integrated with SAINT and a multi-scan absorption correction using SADABS was applied.[19,20] The structures were solved by direct methods using SHELXT and refined by full-matrix least-squares methods against F^2 by SHELXL-2019/2.[21,22] All non-hydrogen atoms were refined with anisotropic displacement parameters. All hydrogen atoms were refined isotropic on calculated positions using a riding model with their U_{iso} values constrained to 1.5 times the U_{eq} of their pivot atoms for terminal sp^3 carbon atoms and 1.2 times for all other carbon atoms. Disordered moieties were refined using bond lengths restraints and displacement parameter restraints. Crystallographic data for the structures reported here have been deposited with the Cambridge Crystallographic Data Centre.[23] CCDC 2383359, 2383360 and 2402128† contain the supplementary crystallographic data for this paper. Reports in the ESI† and the CIF files were generated using FinalCif.[24]

Theoretical calculations

All DFT calculations were performed with ORCA 4.1.2 program package.[25,26] Atom-pairwise dispersion corrections were used for all reported calculations (D3BJ).[27,28] All geometries were obtained *via* optimisation with PBE0/def2-SVP for all carbon and hydrogen atoms while all other atoms were treated with the PBE0/def2-TZVP level of theory and confirmed to be local minima by frequency calculations (no imaginary frequencies).[29–32] Verytight convergence criteria in the SCF procedure and structure optimisation and a fine integration grid (Grid(X)4) were applied. For Ta, the respective build-in effective core potential (ECP) of the ORCA program package was used. Single point calculations were performed on the PBE0/def2-TZVP level of theory for all atoms with a very fine integration grid (Grid(X)6). The RIJCOSX approximation was used in all cases for computational efficiency.[33] Energies in solution were obtained *via* utilisation of a conductor solvent model (CPCM).[34] QTAIM results were obtained from Multiwfn.[35] Molecular orbitals and spin densities were visualised with IboView and ChimeraX, respectively.[36,37] Equatorial coordination of the amido substituent in **2** was found to lie 0.8 and 1.2 kcal mol^{-1} higher in energy in the gas phase and benzene, respectively. The free energy of the hydrogen atom was obtained upon calculation of its single point energy and subsequently corrected upon considering its translational and electronic partition function (4.79 kcal mol^{-1}).[38]

Author contributions

S. P. conducted the synthetic work, acquired the spectroscopic data presented in the manuscript and co-wrote the manuscript and ESI.† Ja. A. developed a new large-scale synthesis of ^{H3}**NNN**^{cat}. A. O.-B. recorded the EPR spectrum of **5**. J. A. conceptualised and supervised the project, acquired funding, performed all crystallographic measurements and theoretical calculation and wrote the manuscript and ESI.† All authors have approved the final version of the manuscript.

Data availability

Synthetic procedures, spectroscopic details and computational details can be found in the ESI. Crystallographic datasets have been deposited at the CCDC under 2383359, 2383360 and 2402128.†

Conflicts of interest

There are no conflicts to declare.

Acknowledgements

This work was funded by the Fonds der Chemischen Industrie e.V. Prof. Christian Limberg, Prof. Kallol Ray and the analytical facilities of the Humboldt-Universität zu Berlin are acknowledged for their support. This work was further funded by the Deutsche Forschungsgemeinschaft under Germany's Excellence Strategy–EXC 2008-390540038–UniSysCat. K. R. and A. O.-B. thank the Einstein Foundation Berlin (ESB)—Einstein Center of Catalysis (EC2) for their scholarship and support.

References

1 (*a*) D. G. Nocera, *J. Am. Chem. Soc.*, 2022, **144**, 1069–1081; (*b*) R. G. Agarwal, S. C. Coste, B. D. Groff, A. M. Heuer, H. Noh, G. A. Parada, C. F. Wise, E. M. Nichols, J. J. Warren and J. M. Mayer, *Chem. Rev.*, 2022, **122**, 1–49; (*c*) R. Tyburski, T. Liu, S. D. Glover and L. Hammarström, *J. Am. Chem. Soc.*, 2021, **143**, 560–576; (*d*) S. Y. Reece and D. G. Nocera, *Annu. Rev. Biochem.*, 2009, **78**, 673–699; (*e*) N. S. Lewis and D. G. Nocera, *Proc. Natl. Acad. Sci. U. S. A.*, 2006, **103**, 15729–15735.

2 (*a*) A. Nakada, T. Matsumoto and H.-C. Chang, *Coord. Chem. Rev.*, 2022, **473**, 214804; (*b*) J. I. van der Vlugt, *Top. Organomet. Chem.*, 2021, **68**, 135–179; (*c*) O. R. Luca and R. H. Crabtree, *Chem. Soc. Rev.*, 2013, **42**, 1440–1459.

3 Selected examples: (*a*) J. Mukherjee, N. Ostermann, X. Aniban, I. Safianova, N. Rotthowe, R. Mata and I. Siewert, *Organometallics*, 2023, **42**, 3258–3265; (*b*) B. J. Charette, J. W. Ziller and A. F. Heyduk, *Inorg. Chem.*, 2021, **60**, 5367–5375; (*c*) G. W. Margulieux, S. Kim and P. J. Chirik, *Inorg. Chem.*, 2020, **59**, 15394–15401; (*d*) E. S. Wiedner, M. B. Chambers, C. L. Pitman, R. Morris Bullock, A. J. M. Miller and A. M. Appel, *Chem. Rev.*, 2016, **116**, 8655–8692; (*e*) E. S. Rountree and J. L. Dempsey, *Inorg. Chem.*, 2016, **55**, 5079–5087; (*f*) L. A. Berben, *Chem. – Eur. J.*, 2015, **21**, 2734–2742; (*g*) E. J. Thompson and L. A. Berben, *Angew. Chem., Int. Ed.*, 2015, **54**, 11642–11646; (*h*) J. T. Henthorn, S. Lin and T. Agapie, *J. Am. Chem. Soc.*, 2015, **137**, 1458–1464; (*i*) C. Milsmann, S. P. Semproni and P. J. Chirik, *J. Am. Chem. Soc.*, 2014, **136**, 12099–12107; (*j*) N. Kumar, D. M. Camaionmi, M. Dupuis, S. Raugei and A. M. Appel, *Dalton Trans.*, 2014, **43**, 11803–11806; (*k*) S. Raugei, S. Chen, M.-H. Ho, B. Ginovska-Pangovska, R. J. Rousseau, M. Dupuis, D. L. DuBois and R. Morris Bullock, *Chem. – Eur. J.*, 2012, **18**, 6493–6506; (*l*) F. Lu, R. A. Zarkesh and A. F. Heyduk, *Eur. J. Inorg. Chem.*, 2012, 467–470; (*m*) C. J. Curtis, A. Miedaner, J. W. Raebiger and D. L. DuBois, *Organometallics*, 2004, **23**, 511–516; (*n*) C. J. Curtis, A. Miedaner, W. W. Ellis and D. L. DuBois, *J. Am. Chem. Soc.*, 2002, **124**, 1918–1925; (*o*) W. W. Ellis, A. Miedaner, C. J. Curtis, D. H. Gibson and D. L. DuBois, *J. Am. Chem. Soc.*, 2002, **124**, 1926–1932; (*p*) E. P. Cappellani, S. D. Drouin, G. Jia, P. A. Maltby, R. H. Morris and C. T. Schweitzer, *J. Am. Chem. Soc.*, 1994, **116**, 3375–3388.

4 Recent review articles: (*a*) D. N. Stephens and M. T. Mock, *Eur. J. Inorg. Chem.*, 2024, **27**, e202400039; (*b*) H. Liu, X. Xu, D. Guan and Z. Shao, *Energy Fuels*, 2024, **38**, 919–931;

(*c*) N. Kostopoulos, M. Robert and A. Sekretareva, *ChemElectroChem*, 2024, **11**, e202300462; (*d*) H.-Y. Liu, H. M. C. Lant, C. C. Cody, J. Jelušić, R. H. Crabtree and G. W. Brudvig, *ACS Catal.*, 2023, **13**, 4675–4682; (*e*) P. L. Dunn, B. J. Cook, S. I. Johnson, A. M. Appel and R. M. Bullock, *J. Am. Chem. Soc.*, 2020, **142**, 17845–17858; (*f*) N. M. Adli, H. Zhang, S. Mukherjee and G. Wu, *J. Electrochem. Soc.*, 2018, **165**, J3130; (*g*) Y. Nishibayashi, *Inorg. Chem.*, 2015, **54**, 9234–9247.

5 (*a*) S. J. K. Forrest, B. Schluschaß, E. Y. Yuzik-Klimova and S. Schneider, *Chem. Rev.*, 2021, **121**, 6522–6587; (*b*) Y. Tanabe and Y. Nishibayashi, *Chem. Soc. Rev.*, 2021, **50**, 5201–5242; (*c*) F. Masero, M. A. Perrin, S. Dey and V. Mougel, *Chem. – Eur. J.*, 2021, **27**, 3892–3928; (*d*) M. J. Bezdek, I. Pappas and P. J. Chirik, *Top. Organomet. Chem.*, 2017, **60**, 1–21; (*e*) Y. Ishida and H. Kawaguchi, *Top. Organomet. Chem.*, 2017, **60**, 45–69.

6 (*a*) N. G. Boekell and R. A. Flowers, *Chem. Rev.*, 2022, **122**, 13447–13477; (*b*) K. T. Tarantino, D. C. Miller, T. A. Callon and R. R. Knowles, *J. Am. Chem. Soc.*, 2015, **137**, 6440–6443.

7 Selected examples: (*a*) C. C. Almquist, N. Removski, T. Rajeshkumar, B. S. Gelfand, L. Maron and W. E. Piers, *Angew. Chem., Int. Ed.*, 2022, **61**, e202203576; (*b*) S. I. Johnson, S. P. Heins, C. M. Klug, E. S. Wiedner, R. M. Bullock and S. Raugei, *Chem. Commun.*, 2019, **55**, 5083–5086; (*c*) M. J. Bezdek and P. J. Chirik, *Angew. Chem., Int. Ed.*, 2018, **57**, 2224–2228; (*d*) G. W. Margulieux, M. J. Bezdek, Z. R. Turner and P. J. Chirik, *J. Am. Chem. Soc.*, 2017, **139**, 6110–6113; (*e*) P. Bhattacharya, Z. M. Heiden, E. S. Wiedner, S. Raugei, N. A. Piro, W. S. Kassel, R. M. Bullock and M. T. Mock, *J. Am. Chem. Soc.*, 2017, **139**, 2916–2919; (*f*) M. J. Bezdek, S. Guo and P. J. Chirik, *Science*, 2016, **354**, 730–733; (*g*) M. J. Bezdek and P. J. Chirik, *Dalton Trans.*, 2016, **45**, 15922–15930.

8 Selected examples: (*a*) E. A. Boyd and J. C. Peters, *J. Am. Chem. Soc.*, 2023, **145**, 14784–14792; (*b*) Y. Ashida, T. Mizushima, K. Arashiba, A. Egi, H. Tanaka, K. Yoshizawa and Y. Nishibayashi, *Nat. Synth.*, 2023, **2**, 635–644; (*c*) N. G. Boekell, C. O. Bartulovich, S. Maity and R. A. Flowers II, *Inorg. Chem.*, 2023, **62**, 5040–5045; (*d*) E. A. Boyd and J. C. Peters, *J. Am. Chem. Soc.*, 2022, **144**, 21337–21346; (*e*) A. Ramírez-Solis, N. G. Boekell, C. I. León-Pimentel, H. Saint-Martin, C. O. Bartulovich and R. A. Flowers II, *J. Org. Chem.*, 2022, **87**, 1689–1697; (*f*) C. O. Bartulovic and R. A. Flowers II, *Dalton Trans.*, 2019, **48**, 16142–16147; (*g*) T. V. Chciuk, W. R. Anderson Jr. and R. A. Flowers II, *J. Am. Chem. Soc.*, 2018, **140**, 15342–15352; (*h*) S. S. Kolmar and J. M. Mayer, *J. Am. Chem. Soc.*, 2017, **139**, 10687–10692; (*i*) T. V. Chciuk, W. R. Anderson Jr. and R. A. Flowers II, *Organometallics*, 2017, **36**, 4579–4583; (*j*) T. V. Chciuk, W. R. Anderson Jr. and R. A. Flowers II, *J. Am. Chem. Soc.*, 2016, **138**, 8738–8741; (*k*) T. V. Chciuk and R. A. Flowers II, *J. Am. Chem. Soc.*, 2015, **137**, 11526–11531.

9 (*a*) R. F. Munhá, R. A. Zarkesh and A. F. Heyduk, *Inorg. Chem.*, 2013, **52**, 11244–11255; (*b*) A. F. Heyduk, R. A. Zarkesh and A. I. Nguyen, *Inorg. Chem.*, 2011, **50**, 9849–9863; (*c*) A. I. Nguyen, K. J. Blackmore, S. M. Carter, R. A. Zarkesh and A. F. Heyduk, *J. Am. Chem. Soc.*, 2009, **131**, 3307–3316; (*d*) R. A. Zarkesh, J. W. Ziller and A. F. Heyduk, *Angew. Chem., Int. Ed.*, 2008, **47**, 4715–4741.

10 J. Underhill, E. S. Yang, T. Schmidt-Räntsch, W. K. Myers, J. M. Goicoechea and J. Abbenseth, *Chem. – Eur. J.*, 2023, **29**, e202203266.

11 C. F. Matta and R. J. Boyd, *in The Quantum Theory of Atoms in Molecules*, John Wiley & Sons, Ltd, 2007, pp. 1–34.

12 P. Coburger, A. Guilherme Buzanich, F. Emmerling and J. Abbenseth, *Chem. Sci.*, 2024, **15**, 6036–6043.

13 V. W. Manner, T. F. Markle, J. H. Freudenthal, J. P. Roth and J. M. Mayer, *Chem. Commun.*, 2008, 256–258.

14 A. Bismuto, P. Müller, P. Finkelstein, N. Trapp, G. Jeschke and B. Morandi, *J. Am. Chem. Soc.*, 2021, **143**, 10642–10648.

15 K. Barral, A. D. Moorhouse and J. E. Moses, *Org. Lett.*, 2007, **9**, 1809–1811.

16 G. Editors John Arnold, P. Scott, K. Nomura, J. Liu, M. S. Hill, M. Hodgson, D. J. Liptrot, M. F. Mahon, N. C. Tomson, J. Arnold, R. G. Bergman, A. Sattler, S. Ruccolo and G. Parkin, *Dalton Trans.*, 2011, **40**, 7777–7782.

17 M. Brookhart, B. Grant and A. F. Volpe, *Organometallics*, 1992, **11**, 3920–3922.

18 T. L. Fischer, M. A. Tepaske and M. A. Suhm, *Phys. Chem. Chem. Phys.*, 2023, **25**, 11324–11330.

19 *Bruker, SAINT, V8.40B*, Bruker AXS Inc., Madison, Wisconsin, USA.

20 L. Krause, R. Herbst-Irmer, G. M. Sheldrick and D. Stalke, *J. Appl. Crystallogr.*, 2015, **48**, 3–10.

21 G. M. Sheldrick, *Acta Crystallogr., Sect. A: Found. Adv.*, 2015, **71**, 3–8, DOI: **10.1107/S2053273314026370**.

22 G. M. Sheldrick, *Acta Crystallogr., Sect. C: Struct. Chem.*, 2015, **71**, 3–8, DOI: **10.1107/S2053229614024218**.

23 C. R. Groom, I. J. Bruno, M. P. Lightfoot and S. C. Ward, *Acta Crystallogr., Sect. B: Struct. Sci., Cryst. Eng. Mater.*, 2016, **72**, 171–179.

24 D. Kratzert, *FinalCif, V139*, **https://dkratzert.de/finalcif.html**.

25 F. Neese, *Wiley Interdiscip. Rev.: Comput. Mol. Sci.*, 2012, **2**, 73–78.

26 F. Neese, *Wiley Interdiscip. Rev.: Comput. Mol. Sci.*, 2017, **8**, e1327.

27 S. Grimme, S. Ehrlich and L. Goerigk, *J. Comput. Chem.*, 2011, **32**, 1456–1465.

28 S. Grimme, J. Antony, S. Ehrlich and H. Krieg, *J. Chem. Phys.*, 2010, **132**, 154104.

29 M. Ernzerhof and G. E. Scuseria, *J. Chem. Phys.*, 1999, **110**, 5029–5036.

30 F. Weigend and R. Ahlrichs, *Phys. Chem. Chem. Phys.*, 2005, **7**, 3297.

31 F. Weigend, *Phys. Chem. Chem. Phys.*, 2006, **8**, 1057.

32 F. Weigend and R. Alrichs, *Phys. Chem. Chem. Phys.*, 2005, **7**, 3297.

33 B. Helmich-Paris, B. de Souza, F. Nesse and R. Izsák, *J. Chem. Phys.*, 2021, **155**, 104109.
34 V. Barone and M. Cossi, *J. Phys. Chem. A*, 1998, **102**, 1995–2001.
35 T. Lu and F. Chen, *J. Comput. Chem.*, 2012, **33**, 580–592.
36 G. Knizia and J. E. M. N. Klein, *Angew. Chem., Int. Ed.*, 2015, **54**, 5518–5522.
37 E. C. Meng, T. D. Goddard, E. F. Pettersen, G. S. Couch, Z. J. Pearson, J. H. Morris and T. E. Ferrin, *Protein Sci.*, 2023, **32**, e4792.
38 N. Alidazeh, J. Abbenseth, S. Bete, M. Finger, M. Otte, C. Würtele and S. Schneider, *Z. Anorg. Allg. Chem.*, 2024, **650**, e202300249.